Two distinct modes in one-day rainfall event during MC3E field campaign: Analyses of disdrometer observations and WRF-SBM simulation

Takamichi Iguchi,[1,2] Toshihisa Matsui,[1,2] Ali Tokay,[2,3] Pavlos Kollias,[4] and Wei-Kuo Tao[2]

[1]   A unique microphysical structure of rainfall is observed by the surface laser optical Particle Size and Velocity (Parsivel) disdrometers on 25 April 2011 during Midlatitude Continental Convective Clouds Experiment (MC3E). According to the systematic differences in rainfall rate and bulk effective droplet radius, the sampling data can be divided into two groups; the rainfall mostly from the deep convective clouds has relatively high rainfall rate and large bulk effective droplet radius, whereas the reverse is true for the rainfall from the shallow wrm clouds. The Weather Research and Forecasting model coupled with spectral bin microphysics (WRF-SBM) successfully reproduces the two distinct modes in the observed rainfall microphysical structure. The results show that the up-to-date model can demonstrate how the cloud physics and the weather condition on the day are involved in forming the unique rainfall characteristic. **Citation:** Iguchi, T., T. Matsui, A. Tokay, P. Kollias, and W.-K. Tao (2012), Two distinct modes in one-day rainfall event during MC3E field campaign: Analyses of disdrometer observations and WRF-SBM simulation, *Geophys. Res. Lett.*, *39*, L24805, doi:10.1029/2012GL053329.

1. Introduction

[2] Precipitation is a key component of earth's energy and water cycle. It is an integral product of hydrometeor size distribution where the size of the hydrometeors ranges from a small drizzle drop (≥ 0.1 mm in diameter) to a hailstone (>10 cm in diameter). Several processes are responsible for determining the size and phase of individual hydrometeors at the surface including but not limited to aerosol loading, liquid water availability, structures of vertical and horizontal wind velocities, presence or absence of mixed-phase processes, and subcloud layer evaporation.

[3] Microphysical structure of precipitation at the ground is of interest in developing cloud microphysical models, in terms of improving forecast accuracy of surface precipitation rate as well as validating cloud microphysics by regarding

precipitation as a product. Bulk cloud microphysics is commonly used in the present atmospheric models; however, there is little room for change in the precipitation microphysics because certain mathematical functions are used as built-in parameterization to represent particle size distribution (PSD). In contrast, spectral bin microphysics (SBM) allows prediction of hydrometeor PSDs and subsequently explicit representation of precipitation microphysical structure. Numerical weather prediction (NWP) simulations using SBM have been utilized mostly in the research field of cloud-aerosol interactions in previous studies [e.g., *Lynn et al.*, 2005]. Analysis and verification of the ground precipitation microphysics can be a new application of the simulation to show possibilities of the up-to-date models.

[4] This paper reports on the analysis of distinct rainfall microphysical structures associated with deep convective system and shallow boundary layer clouds in the rainfall event on 25 April 2011. The event was observed during the Midlatitude Continental Convective Clouds Experiment (MC3E) at the Atmospheric Radiation Measurement (ARM) Southern Great Plains (SGP) site in central Oklahoma. The disdrometer-based observations for raindrop size distribution (DSD) are analyzed to determine the characteristic of the rainfall, which is compared with a simulation result of the Weather Research and Forecasting model coupled with spectral bin microphysics (WRF-SBM).

2. Description of Model Simulation and Overall Condition on 25 April 2011 at SGP Site

[5] The WRF-SBM has been developed for supporting the National Aeronautics and Space Administration (NASA) Global Precipitation Measurement (GPM) mission; the MC3E field campaign is a part of GPM Ground validation (GV) program. The SBM part is the same as the microphysical scheme of the Hebrew University Cloud Model (HUCM) [*Khain et al.*, 2011]. The scheme has been implemented into the Advanced Research WRF (ARW) version 3.1.1 [*Iguchi et al.*, 2012]. Hydrometeors are categorized into one-water and six-ice classes, i.e., water droplets, ice crystals (plate, column, dendrite), snow aggregates, graupel, and hail; the discrete PSDs of the hydrometeor classes are represented on a grid containing 43 doubling mass bins. In order to simulate the entire rainfall event, the simulation domain covers 454×388 horizontal grids domain with 3 km horizontal grid spacing and inner-telescoped 642×498 horizontal grids domain with 1 km grid spacing. The inner domain includes the location of the ARM SGP site. The WRF-SBM was employed in 24-hours real-time forecasting on 25 April 2011 using online 2-way grid nesting configuration for

---
[1]Earth System Science Interdisciplinary Center, University of Maryland, College Park, Maryland, USA.
[2]Laboratory for Atmospheres, NASA Goddard Space Flight Center, Greenbelt, Maryland, USA.
[3]Joint Center for Earth Systems Technology, University of Maryland, Baltimore County, Baltimore, Maryland, USA.
[4]Department of Atmospheric and Oceanic Sciences, McGill University, Montreal, Quebec, Canada.

Corresponding author: T. Iguchi, Laboratory for Atmospheres, NASA Goddard Space Flight Center, Code 612, Greenbelt, MD 20771, USA. (takamichi.iguchi@nasa.gov)
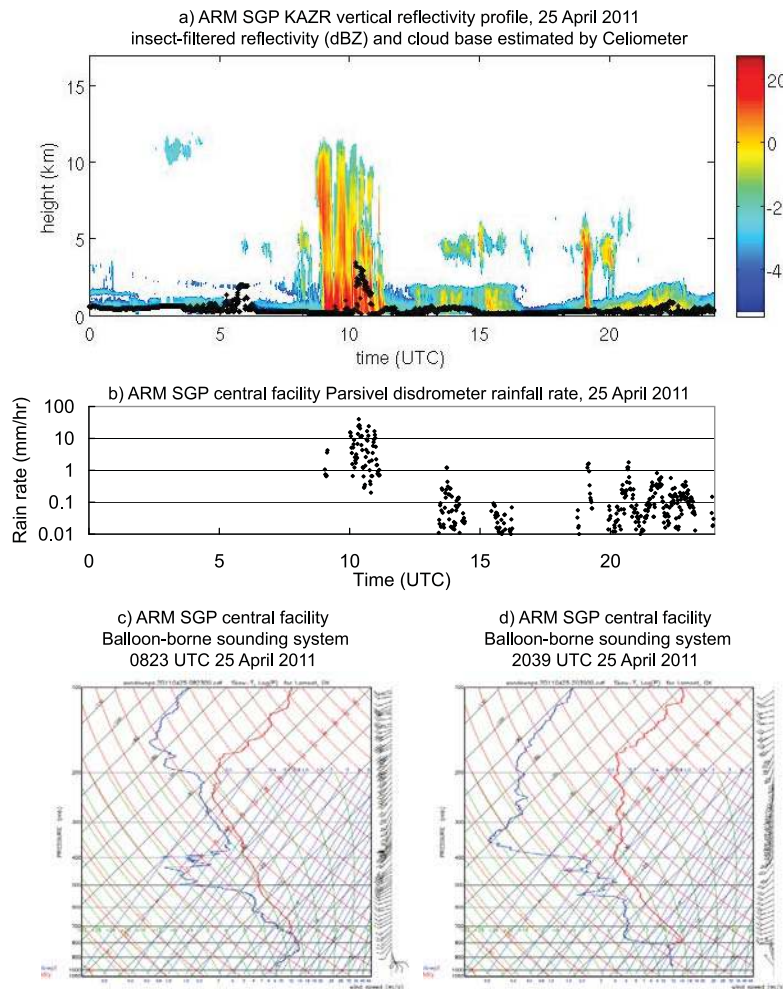
Figure 1. Time series of (a) the Ka-band ARM Zenith Radar (KAZR) vertical reflectivity profile and (b) the rainfall rate measured by the laser optical Parsivel disdrometer over ARM SGP central facility (C1) site on 25 April 2011. Balloon-borne sounding at C1 site at (c) 0823 UTC and (d) 2039 UTC.

the two domains (detailed information can be found in auxiliary material).[1]

[6] The Ka-band ARM Zenith Radar (KAZR) observations [e.g., *Clothiaux et al.*, 2000; *Kollias et al.*, 2007] at the SGP central facility site show that a series of deep convective clouds with the cloud top heights up to 10 km passed over the site from 09 UTC to 11 UTC on 25 April 2011 (Figure 1a). High rainfall rate up to approximately 40 mm hr^{-1} was observed by the collocated laser optical Particle Size and Velocity (Parsivel) disdrometer during this period (Figure 1b). On the other hand, shallow boundary layer clouds less than the height of 2 km continuously hanged over the site, and weak rainfall approximately 1 mm hr^{-1} was observed intermittently from 13 UTC to 23 UTC. The atmospheric thermodynamics structure captured by the radiosonde data collected at the SGP site at 08 and 23 UTC (Figures 1c and 1d) indicates several features related to the aforementioned precipitation activity. A capping inversion of temperature was observed under freezing (0°C) level with humid

boundary layer. As a result, shallow warm clouds were most likely to be formed under the conditions limiting vertical development of clouds. However, cold deep layer in conditional instability is observed above 0°C level in the free atmosphere. Deep convections thus tended to be easily formed when once strong convection is triggered through the capping inversion.

3. Results

3.1. Surface Rainfall Structure: Comparison Between the Disdrometer Measurements and Simulation

[7] Laser optical Parsivel disdrometers [*Löffler-Mang and Joss*, 2000] were installed at 16 locations around the ARM SGP central site (36.36°N, 97.29°W) (Figure S1). The maximum distance between these disdrometers was 12.26 km. The disdrometers had a sampling of the maximum length of the falling particle in a horizontal plane and sorted particles into a matrix of 32 size intervals ranging 0 to 26.78 mm and 32 fall velocity intervals ranging from 0.05 to 20.8 m s^{-1}; the contents in the first and second size intervals ($D < 0.26$ mm) were cut-off because of large noise for small detection. The

data was recorded per 10 seconds and integrated to 1 minute. The DSD from Parsivel is determined from raw 32×32 size versus fall velocity matrix and is expressed as a function of drop diameter, D (mm):

$$N(D_j) = \frac{1}{\Delta t} \cdot \frac{C_j}{v(D_j) Area \Delta D_j}, \qquad (1)$$

where j is the index of the diameter bin, Δt is observation period in seconds, $Area$ is the cross-sectional area, which is nominally 54 cm^2 since length and width of the laser beam are 180 mm and 30 mm, respectively. But it is expressed as a function of D (length $\times$ [width $-$ ($D_j/2$)]) to account partially observed drops that are at the edge of the laser beam. ΔD_j is the bin width, C_j is the number of drops at a given size bin and measured fall velocity, $v(D_j)$.

[8] Integral rainfall parameters, i.e., total number concentration, N_t (drops m^{-3}), bulk raindrop effective radius, r_e (μm), rainfall rate, R (mm hr^{-1}), radar reflectivity, Z (mm^6 m^{-3}), are calculated by integrating DSD spectra as follows:

$$N_t = \frac{1}{\Delta t} \sum_{j=1}^{32} \frac{C_j}{v(D_j) Area}, \qquad (2)$$

$$r_e = \frac{10^3 \sum_{j=1}^{32} D_j{}^3 N(D_j) \Delta D_j}{2 \sum_{j=1}^{32} D_j{}^2 N(D_j) \Delta D_j}, \qquad (3)$$

$$R = \frac{6\pi \times 10^{-4}}{\Delta t} \sum_{j=1}^{32} \frac{C_j D_j{}^3}{Area}, \qquad (4)$$

$$Z = \sum_{j=1}^{32} D_j{}^6 N(D_j) \Delta D_j. \qquad (5)$$

Figures 2a and 2c show scatter diagrams of $N_t(D > 0.77$ mm)-R and r_e-R correlations derived from the 15 Parsivel measurements (the data of one unit was corrupted) for 24 hours on 25 April 2011. Note that N_t is calculated using parts of DSDs with $D > 0.77$ mm in consideration of possible underestimation of number concentration at the small size range in Parsivel measurements [Tokay et al., 2001]. The plots are color-coded for the period from 06 to 12 UTC in blue and from 03 to 06 and from 12 to 24 UTC in red; this grouping is based on the difference in approximate time of passages of the deep convective system and shallow boundary layer clouds. The groups of the blue- and red-color dots can be recognized as two distinct modes characterized by large r_e and R and small r_e and R, respectively (Figure 2c). The threshold value of r_e is approximately 400 μm, and R ranges from 0.01 to 10 mm hr^{-1} and from 0.1 to 100 mm hr^{-1} in each group. On the other hand, Figure 2a shows that N_t group of the blue-color marks branches off with slightly smaller N_t from the red-color group at approximately $R = 1$ mm hr^{-1}, while both modes has a monotonous increase in R at log-scale with a similar increase in N_t up to 1000 m^{-3}. This behavior is

related to difference in r_e. In the red-color group, small and almost constant r_e suppresses an increase in R heavier than 10 mm hr^{-1}. In contrast, R increases up to 100 mm hr^{-1} with an increase in r_e in the blue-color group. The existence of the two distinct modes for correlation between particle size and rainfall rate can be justified by the 2-dimensional video disdrometer (2DVD) measurements for the same rainfall event (Figure S2b).

[9] In order to obtain the corresponding precipitation DSDs by the disdrometric measurement and subsequently integral rainfall parameters from the WRF-SBM simulation, so-called Parsivel simulator was designed: Momentary 43 binned PSDs of the WRF-SBM simulation were recorded per hour for all model grid points. Then, surface 32-binned precipitation DSD (equation (1)) was calculated using the 43-binned PSDs and terminal fall velocities for mass bins in the SBM. The binned size ranges of the 32 bins were identical to those used in the Parsivel disdrometer program. The contents in the first and second bins ($D < 0.26$ mm) were cut-off to be aligned with the actual disdrometer sampling. Then, the corresponding integral rainfall parameters were calculated following equations (1)–(5). This approach allows a reasonable straightforward comparison of rainfall parameters between the simulation and measurement, though uncertainty due to the incompatibility of sampling timing and location remains. The integral parameters were sampled over a domain of 20 km square centered at the ARM SGP site. The application of longer distance than the maximum distance between the distrometers is to fill up the difference in number of sampling between the measurements and simulation with different sampling intervals.

[10] Figures 2b and 2d show scatter diagrams of $N_t(D > 0.77$ mm)-R and r_e-R correlations derived from the WRF-SBM simulation. The plots are color-coded for the period from 06 to 12 UTC in blue and from 03 to 05 and from 13 to 24 UTC in red (the reason of the different notations between the measurements and simulation is because the momentary output of the simulation was recorded per hour). The simulation reproduced overall two distinct characteristics of N_t-R and r_e-R that correspond reasonably well with those in the observed plots: Branch off of the blue-color marks group from the red-color group is simulated at $R > 1$ mm hr^{-1} (Figure 2b). Two distinct modes characterized by large r_e and R (blue) and small r_e and R (red) are simulated (Figure 2d). However, the simulated plots pattern are more scattered than that of the measurements. In particular, difference in r_e between the measurements and simulation is highlighted at $R < 1$ mm hr^{-1}; the simulated r_e is scattered to larger value in both color groups. The overprediction of r_e at the small R range is caused by a group of DSD with small N_t less than 0.5 m^{-3}, seen only in the simulation plot (Figure S3). The marks with overprediction of r_e can be almost removed by sampling only DSDs with N_t larger than 0.5 m^{-3} (Figure S4). Although the distrometers may capture DSDs with the tiny N_t, they are disregarded as noise [Tokay et al., 2005]. The set of large r_e, small N_t and R is simulated at grids probably where rainfall begins to fall and only large raindrops reach to the surface in advance. Spontaneous breakup of large drops is not considered in the present SBM, so that huge raindrops after melting of huge ice particles like hailstones may artificially reach to the ground without breakup and be sampled in the simulation.
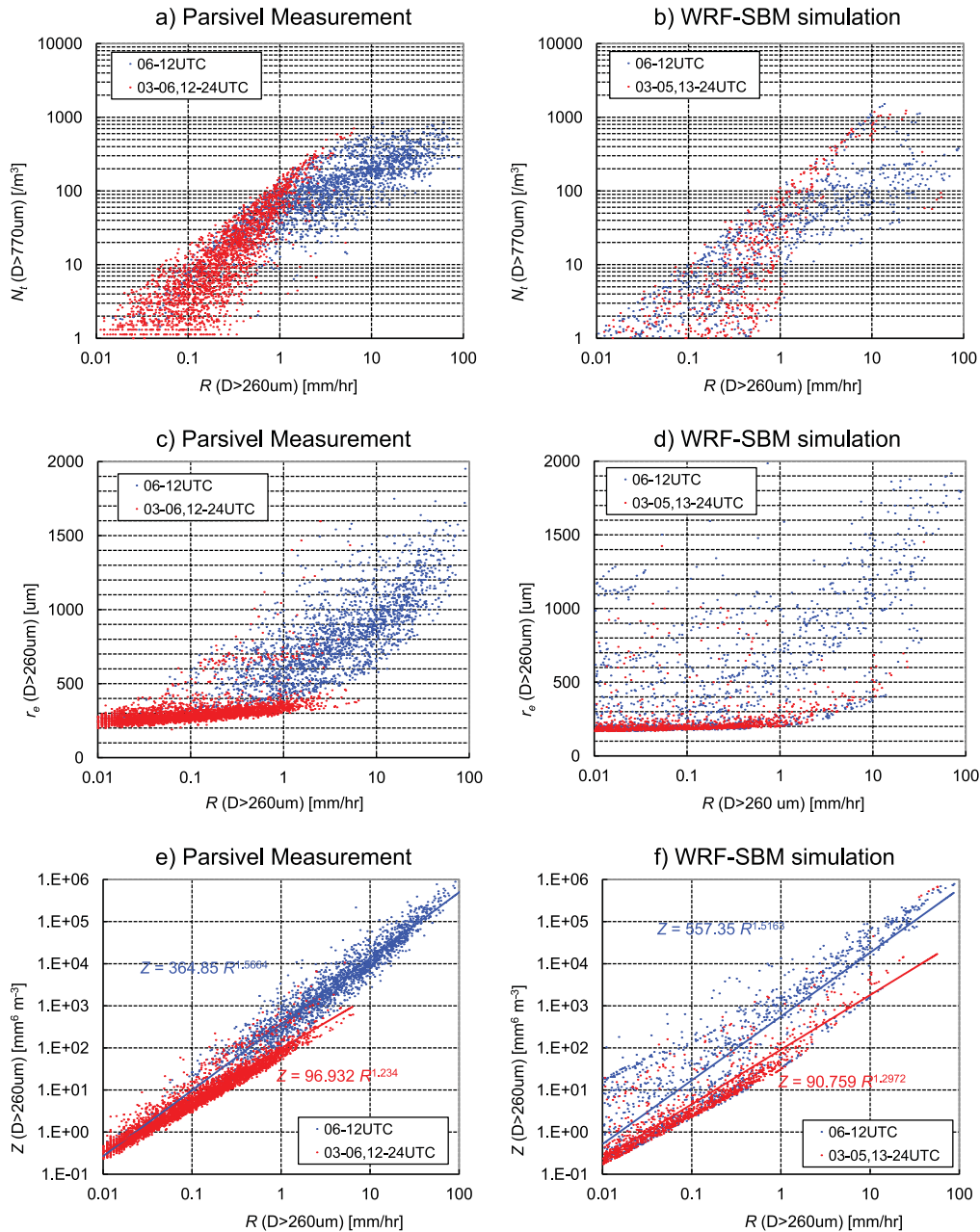
Figure 2. Scatter diagrams (a, b) between N_t and R, (c, d) between r_e and R derived from the disdrometric observational data and from the WRF-SBM simulation result, and (e, f) between Z and R, derived from the disdrometric observational data and from the WRF-SBM simulation result. Plots are color-coded by the sampling period, 06–12 UTC (blue) and 03–06, 12–24 UTC (red) for the measurements and 03–05, 13–24 UTC (red) for the simulation. Lines and equations in Figures 2e and 2f show the fitted lines approximating a power function and the approximate equations for each color group, respectively.

[11] The relationship between Z and R is generally approximated to be a form of a power law function, $Z = AR^b$. The values of the coefficients are recognized as an important aspect of the rainfall characteristics, though the values have non-negligible dependency on the types of measurement instruments and the regression techniques [*Campos and Zawadzki*, 2000; *Tokay et al.*, 2001]. Figures 2e and 2f illustrate the Z-R relationships in the form of scatter diagrams derived from the measurements and simulation, respectively. The parameters, A and b, are computed using a linear regression method separately for the plot groups of

red-color and blue-color, shown in the form of $Z = AR^b$ in the panels. The values of A and b of the simulation are generally good agreement with those of the observation, except for A for the blue-colored dots. This difference is considered to be due to the same source as in the aforementioned difference in r_e at the range of $R < 1$ mm hr^{-1}.

[12] The timing of appearances of convective and stratiform clouds around the SGP site in the simulation is justified by the overall agreement between the observation and simulation panels in Figure 2, though the present grouping according to the time ranges may be coarse. Shallow
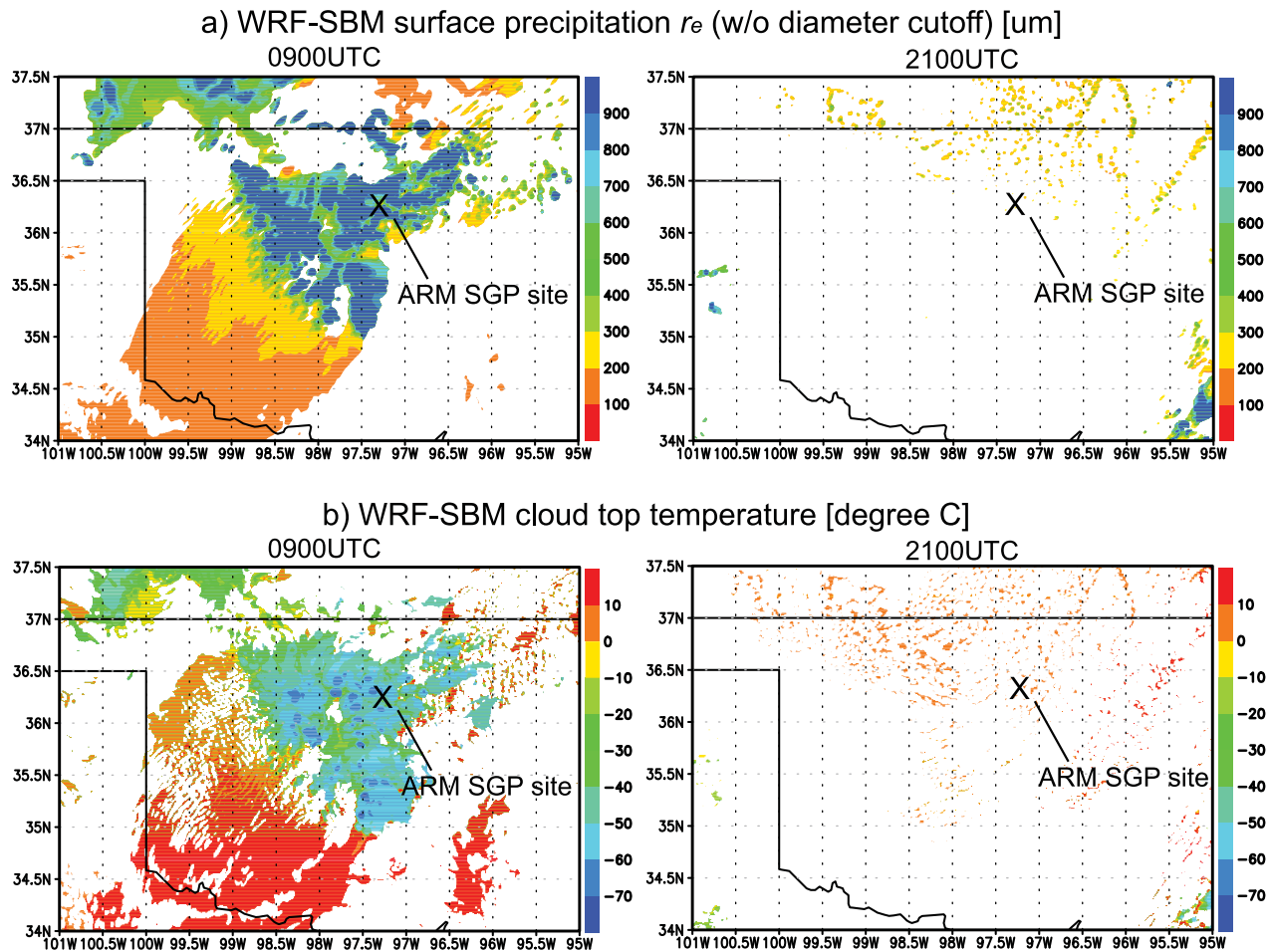
Figure 3. Snapshots of horizontal distributions of (a) surface precipitation r_e (without diameter cutoff) and (b) cloud-top temperature of the WRF-SBM simulation at (left) 09 and (right) 21 UTC on 25 April 2011.

boundary clouds with rainfall, however, seem to be over-simulated and included in the 06–12 UTC group as compared to the measurements, because a non-neglectable part of blue-color marks are overlapped by the red-color marks in the simulation panels of Figure 2.

3.2. Relationship Between the Surface Rainfall Structures and the Cloud/Weather Conditions

[13] These distinct rainfall characteristics originated from difference in processes between the deep convective and shallow boundary layer clouds to form the precipitation. Figure 3 illustrates the horizontal distributions of r_e (without cutoff at particular diameter for surface DSD) and cloud-top temperature, derived from the WRF-SBM simulation at 09 and 21 UTC; the cloud-top temperature is here defined as air temperature at the highest model level containing the total water content larger than 0.3 g m^{-3} in each grid column. This figure clearly demonstrates that r_e and the cloud-top temperature are inversely correlated. In particular, a boundary around 400 μm of r_e in Figure 3a is in good agreement with a border of 0° Celsius of the cloud-top temperature in Figure 3b. These results show that the surface precipitation of red- and blue-color groups in Figure 2 mostly originates from shallow warm and deep mixed-phase rain processes, respectively.

[14] At 09 UTC (Figure 3, left), couples of deep convective system are simulated over the ARM SGP site. The coldest cloud-top temperature is approximately −60°C, and the corresponding surface DSD r_e is more than 900 μm (up to 2000 μm as shown in Figure 2d). Shallow warm clouds with the cloud-top temperature over 0°C cover the wide area of southwestern segment and move toward the ARM SGP site by a southwestern wind. The r_e of the shallow system is approximately 300 μm. At 21 UTC (right panels), a number of patchy shallow clouds remain over area including the location of ARM SGP site. The r_e is approximately 300–400 μm. The simulated cloud top heights over the site at 09 and 21 UTC are in reasonably agreement with those observed by the KAZR (Figure 1a). The WRF-SBM simulation poorly reproduced the homogenous distribution of shallow stratiform clouds at 21 UTC, which is speculated by the KAZR profile around the time. An accurate prediction of cloud fraction is a difficult problem even in a high-resolutional simulation [e.g., *Khairoutdinov and Randall*, 2003], and this problem needs to be investigated more in future works.

[15] In the case on 25 April, 0°C temperature level were located at a height of approximately 3.5 km, so that warm clouds below this level were shallow and raindrops reached to the ground from clouds immediately. Terminal fall velocity with droplet radius of 400 μm is assumed to be

approximately 2.6 m s^{-1} at 1000 hPa level in the model microphysics [*Khain and Sednev*, 1995]. Against this fall velocity, maximum updraft velocity in the simulated shallow warm clouds is roughly 2 m s^{-1}. Thus, particles that grow larger up to the radius of approximately 400 μm cannot be held in the clouds and fall to the ground. The small updraft velocity in the shallow clouds is a factor of small surface r_e. On the other hand, 10 m s^{-1} or much stronger updraft velocities in the deep convective system were simulated, so that any size particles in the model can be held in the updraft region of the clouds. Thus, much larger particles than those from the shallow warm clouds can be generated and finally fall to the ground. The surface rainfall rate increases with an increase in surface-rainfall r_e.

[16] Figure S5a illustrates the simulated thermodynamic fields that cause the formation of series of deep convective clouds at 09 UTC, which corresponds to those observed by the KAZR (Figure 1a). There are two major flows of warm, moist air from the southern part and cold, dry air from the northern part on 850 hPa level. Parts of the two major flows are converged around 36°N, 98°W. This is approximately the center of the deep convective system. A couple of warm cores are formed around the coordinates on the 850 hPa pressure level. Warm air mass is transported to the level of free atmosphere in conditional instability, and induces deep convections. On a north-south cross-section of the east-side of the system along 97.5°W (Figure S5b), a strong vertical wind shear is simulated under 800 hPa level. A low-level flow from south rises to a higher level at 35°N by the opposite wind, and then air mass diverges at the top of deep convection, approximately on 200 hPa level. Deep convections are continuously induced along the outflow boundaries originating from the convection close behind. The deep convective system is conveyed northeastward by the background southwestern wind.

[17] On the other hand, shallow boundary layer clouds are simulated over the southwestern segment at 09 UTC. Nocturnal boundary layer clouds are often observed over this area, and the detailed mechanism was investigated in *Zhu et al.* [2001]. Turbulence driven by wind shear is an important factor to maintain well-mixed boundary layer and form clouds, in place of radiative heating in daytime. Figure S5c shows that shallow clouds are simulated along remarkable wind shear near the ground. Relative humidity reaches 100% and condensation occurs under or around capping inversion of temperature (Figure S6). Unlike the segment shown in Figure S5b, deep convective system are not developed, probably because of no convergence promoting breakup of the capping and subsequently involvement in free atmosphere with conditional instability. The boundary layer structure shown in Figure S6 is similar to those observed at ARM SGP site before and after the passage of the deep convective system (Figures 1c and 1d). These results imply that the observed soundings at the times are under a sufficient condition to form shallow boundary layer clouds.

4. Conclusions

[18] We have analyzed the Parsivel disdrometer observations at the ARM SGP site on 25 April, 2011. The measurement results show unique distinctive structures of correlations between the integral rainfall parameters, which can be classified into two groups mostly according to the types of clouds causing the precipitation. The group with large bulk effective particle size and rainfall rate originates from series of deep convective clouds, whereas the inverse is true for the group from shallow boundary layer clouds. The WRF-SBM weather prediction simulation could successfully reproduce the rainfall microphysical structures. The simulation for high rainfall rate is well, whereas the low rate rainfall is simulated relatively with defects; note that the measurements also have a large uncertainty at low rainfall rate, especially $R < 0.1$ mm/hr. The discussion on the surface rainfall microphysics was expanded to relevance to the weather and cloud conditions on the day, by referring to the three-dimensional atmospheric field in the simulation. The simulation demonstrated that the horizontal distribution of the classified precipitation was well inversely correlated with that of cloud-top temperature; that is, the distinct rainfall structures are derived from the difference between the deep mixed-phase and shallow warm rain processes in clouds aloft. The characteristic structures of cloud and precipitation were most likely to be formed under the weather condition on the day. Series of deep convective clouds were locally and rapidly developed through meso-scale feedback process. Shallow boundary layer clouds were easily formed under the atmospheric sounding with humid boundary layer under temperature inversion.

[19] This paper has presented a possibility of the high-resolution NWP simulation coupled with one of the up-to-date microphysical schemes, even though this is a single case study for one-day precipitation event. This rainfall event is set as an important case in the MC3E field campaign during April and May 2011. The three-dimensional output including hydrometeor PSDs of the WRF-SBM is planned to be provided to the MC3E and GPM science communities to support their research, e.g., for testing/developing the GPM pre-launch precipitation retrieval algorithm.

References

Campos, E., and I. Zawadzki (2000), Instrument uncertainties in Z–R relations, *J. Appl. Meteorol.*, 39, 1088–1102, doi:10.1175/1520-0450(2000) 039<1088:IUIZRR>2.0.CO;2.

Clothiaux, E. E., T. P. Ackerman, G. G. Mace, K. P. Moran, R. T. Marchand, M. A. Miller, and B. E. Martner (2000), Objective determination of cloud heights and radar reflectivities using a combination of active remote sensors at the ARM CART sites, *J. Appl. Meteorol.*, 39, 645–665, doi:10.1175/1520-0450(2000)039<0645:ODOCHA>2.0.CO;2.

Iguchi, T., T. Matsui, J. J. Shi, W.-K. Tao, A. P. Khain, A. Hou, R. Cifelli, A. Heymsfield, and A. Tokay (2012), Numerical analysis using WRF-SBM for the cloud microphysical structures in the C3VP field campaign: Impacts of supercooled droplets and resultant riming on snow microphysics, *J. Geophys. Res.*, doi:10.1029/2012JD018101, in press.

Khain, A., A. Pokrovsky, D. Rosenfeld, U. Blahak, and A. Ryzhkov (2011), The role of CCN in precipitation and hail in a mid-latitude storm as seen in simulations using a spectral (bin) microphysics model in a 2D dynamic frame, *Atmos. Res.*, 99, 129–146, doi:10.1016/j.atmosres.2010.09.015.

Khain, A. P., and I. L. Sednev (1995), Simulation of hydrometeor size spectra evolution by water-water, ice-water and ice-ice interactions, *Atmos. Res.*, 36, 107–138, doi:10.1016/0169-8095(94)00030-H.

Khairoutdinov, M. F., and D. A. Randall (2003), Cloud resolving modeling of the ARM summer 1997 IOP: Model formulation, results, uncertainties,

and sensitivities, *J. Atmos. Sci.*, *60*, 607–625, doi:10.1175/1520-0469 (2003)060<0607:CRMOTA>2.0.CO;2.

Kollias, P., M. A. Miller, E. P. Luke, K. L. Johnson, E. E. Clothiaux, K. P. Moran, K. B. Widener, and B. A. Albrecht (2007), The Atmospheric Radiation Measurement Program cloud profiling radars: Second-generation sampling strategies, processing, and cloud data products, *J. Atmos. Oceanic Technol.*, *24*, 1199–1214, doi:10.1175/JTECH2033.1.

Löffler-Mang, M., and J. Joss (2000), An optical disdrometer for measuring size and velocity of hydrometeors, *J. Atmos. Oceanic Technol.*, *17*, 130–139, doi:10.1175/1520-0426(2000)017<0130:AODFMS>2.0.CO;2.

Lynn, B. H., A. P. Khain, J. Dudhia, D. Rosenfeld, A. Pokrovsky, and A. Seifert (2005), Spectral (bin) microphysics coupled with a mesoscale

Model (MM5). Part I: Model description and first results, *Mon. Weather Rev.*, *133*(1), 44–58, doi:10.1175/MWR-2840.1.

Tokay, A., A. Kruger, and W. F. Krajewski (2001), Comparison of drop size distribution measurements by impact and optical disdrometers, *J. Appl. Meteorol.*, *40*, 2083–2097, doi:10.1175/1520-0450(2001) 040<2083:CODSDM>2.0.CO;2.

Tokay, A., P. G. Bashor, and K. R. Wolff (2005), Error characteristics of rainfall measurements by collocated Joss-Waldvogel disdrometers, *J. Atmos. Oceanic Technol.*, *22*, 513–527, doi:10.1175/JTECH1734.1.

Zhu, P., B. A. Albrecht, and J. Gottschalck (2001), Formation and development of nocturnal boundary layer clouds over the southern Great Plains, *J. Atmos. Sci.*, *58*, 1409–1426, doi:10.1175/1520-0469(2001)058<1409: FADONB>2.0.CO;2.